Applied Catalysis B: Environmental 130–131 (2013) 73–83

Contents lists available at SciVerse ScienceDirect

Applied Catalysis B: Environmental

journal homepage: www.elsevier.com/locate/apcatb

Improving the DME steam reforming catalyst by alkaline treatment of the HZSM-5 zeolite

Jorge Vicente, Ana G. Gayubo, Javier Ereña*, Andrés T. Aguayo, Martin Olazar, Javier Bilbao

Departamento de Ingeniería Química, Universidad del País Vasco UPV/EHU, Apartado 644, 48080 Bilbao, Spain

ARTICLE INFO

Article history:
Received 12 July 2012
Received in revised form 15 October 2012
Accepted 22 October 2012
Available online 1 November 2012

Keywords:
Dimethyl ether
Hydrogen
Steam reforming
HZSM-5 zeolite
Alkaline treatment

ABSTRACT

Dimethyl ether (DME) steam reforming for hydrogen production has been studied on a bifunctional catalyst prepared by the (wet) physical mixing (at 50 wt%) of a metallic function of CuO–ZnO–Al_2O_3 (Cu/Zn/Al atomic ratio = 4.5:4.5:1.0, prepared by co-precipitation) and an acidic function of HZSM-5 zeolite modified by alkaline treatments of different severity. The runs have been carried out in a fluidized bed reactor. The results obtained by using treated HZSM-5 zeolites and γ-Al_2O_3 as acid functions have been compared. The alkaline treatment affects both the acid properties of the zeolite (attenuating total acidity and acid strength) and its porous structure (increasing the mesoporous surface and decreasing the microporous volume and BET surface area). The attenuation in acidity hinders the formation of undesired hydrocarbons from oxygenates (methanol + DME). Consequently, alkaline treatment (with 0.2–0.4 M NaOH solutions for 300 min) is suitable for improving the kinetic performance of the bifunctional catalyst, as it provides high selectivity and a high yield of H_2 at 300 °C without hydrocarbon formation, as well as minimizing CO formation and avoiding deactivation by Cu sintering. The catalyst is stable, and its kinetic performance remains constant throughout long runs.

1. Introduction

Hydrogen is considered a suitable fuel to meet ever-increasing energy demand because it may be produced from renewable sources [1]. Hydrogen fuel cells are presented as an efficient and environmentally friendly power generator applicable to both mobile and stationary use [2]. Although hydrogen has a high fuel density, it is difficult to handle and, therefore, a hydrogen vector (e.g., methanol, ethanol, gasoline, diesel and methane) needs to be used for H_2 production for fuel cell processors by means of reforming processes.

Methanol can be easily and selectively converted into an H_2-rich gas at low temperature (150–300 °C) by steam reforming [3] and, therefore, it is an excellent raw material for on-board H_2 production for PEM fuel cells. However, the infrastructure for processing methanol is not well developed and methanol toxicity is high. The reforming of dimethyl ether (DME) is an alternative of growing interest [4–11], given that DME is relatively inert, non-corrosive, non-carcinogenic and can be stored and handled as LPG, which means it is more readily used as a fuel and in fuel cells [12]. DME synthesis from syngas in a single step on bifunctional catalysts is thermodynamically more favoured than methanol synthesis and, moreover, CO_2 can be co-fed together with the syngas [13–15]. Accordingly, Olah et al. [16] consider DME synthesis in a single step as a key process for large-scale CO_2 valorization. Furthermore, DME has also attracted increased attention as a clean fuel.

The main reactions in the process of DME steam catalytic reforming are:

DME steam reforming $(CH_3)_2O + 3H_2O \leftrightarrow 6H_2 + 2CO_2$ (1)

DME hydrolysis $(CH_3)_2O + H_2O \leftrightarrow 2CH_3OH$ (2)

MeOH steam reforming $CH_3OH + H_2O \leftrightarrow 3H_2 + CO_2$ (3)

r-WGS $CO_2 + H_2 \leftrightarrow H_2O + CO$ (4)

DME decomposition $(CH_3)_2O \rightarrow CH_4 + H_2 + CO$ (5)

Steam reforming of DME (SRD) (Eq. (1)) consists of two steps in series: DME hydrolysis (Eq. (2)) on an acid function and methanol steam reforming (Eq. (3)) on a metallic function. Apart from SRD, a reverse water-gas shift reaction (r-WGS) (Eq. (4)) usually takes place on the metallic function, and methane is also formed via DME decomposition (Eq. (5)) when a strong acidic function or high temperatures are used [7]. Consequently, suitable metallic and acid functions are required for attaining high DME conversion and high H_2 selectivity by avoiding the formation of CO (poison for the anodic catalyst in PEM fuel cells) and CH_4 as byproducts.

Cu-based catalysts are well known for their high activity for methanol steam reforming and selectivity towards H_2 [17].

* Corresponding author. Tel.: +34 94 6015363; fax: +34 94 6013500.
E-mail address: javier.erena@ehu.es (J. Ereña).

0926-3373/$ – see front matter © 2012 Elsevier B.V. All rights reserved.
http://dx.doi.org/10.1016/j.apcatb.2012.10.019

Nomenclature

A0.2-10, A0.2-300, A0.4-300 HZ30 zeolites treated with 0.2 M NaOH for 10 min, 0.2 M NaOH for 300 min and 0.4 M NaOH for 300 min, respectively
ALU γ-Al_2O_3 acid function
Br Brönsted acid sites
CZA CuO–ZnO–Al_2O_3 metallic function
CZA/ALU, CZA/HZ30, CZA/A0.2-10, CZA/A0.2-300, CZA/A0.4-300 bifunctional catalysts made up of CuO–ZnO–Al_2O_3 and different acid functions: ALU, HZ30 zeolite or zeolites treated with alkali (A0.2-10, A0.2-300, A0.4-300), respectively
$\bar{d}_{Cu}$ average particle size of Cu (Å)
DME dimethyl ether
d_{pore} pore diameter (Å)
DSC digital scanning calorimetry
F_i, $F_{i,0}$ molar flow rate of *i* component at the reactor outlet and in the feed, respectively
GHSV gas hourly space velocity
HC hydrocarbons
HZ30 parent (untreated) HZSM-5 zeolite
Lw Lewis acid sites
MeOH methanol
MTG, MTH, MTO methanol to gasoline, methanol to hydrocarbons and methanol to olefins, respectively
PEM polymer electrolyte membrane
P_i partial pressure of *i* component (bar)
r-WGS reverse water-gas shift reaction
S_{BET} BET surface area of the solid (m^2/g)
$S_{external}$ external surface area of the solid (m^2/g)
$S_{metallic}$ specific metal surface area (m^2 Cu/g Cu)
$S_{micropore}$ micropore surface area (m^2/g)
SRD steam reforming of dimethyl ether
TPD temperature programmed desorption
TPR temperature programmed reduction
$V_{mesopore}$, $V_{micropore}$ mesopore and micropore volume (cm^3/g)
X_{DME} DME conversion
x_i *i* component molar fraction
X_{MeOH} methanol effective conversion in the second step of the SRD process
XRD X-ray diffraction analysis
XRF X-ray fluorescence spectroscopy
Y_i yield of *i* component
υ_i stoichiometric coefficient of *i* component

Accordingly, commercial or laboratory synthesized CuO–ZnO–Al_2O_3 metallic functions have been widely used in the bifunctional catalysts for SRD [6,18–22]. Other Cu-based metallic functions studied for SRD include Cu–CeO_2 [23–25] and Cu–Ni [26]. Noble metal based catalysts, such as Pt/Al_2O_3 or Ru/Al_2O_3, give way to a relatively high DME conversion, although a rather high production of CH_4 is obtained [11]. The formation of CH_4 (up to 25%) can be significantly reduced (to 7%) by mixing Pt/Al_2O_3 catalysts with Pd/Al_2O_3, with no loss in hydrogen production activity [27].

The choice of acid function is essential for the development of catalysts for SRD, given that hydrolysis is the process limiting step. γ-Al_2O_3 is the more commonly used catalyst [4,8–10,18,26,28], but due to its very low acidity, high temperatures (usually in the 300–400 °C range) are required for high DME conversion, with considerable sintering of the Cu metallic function at these temperatures. Spinels have been proposed for improving the stability of Cu metallic functions above 300 °C, and a spinel of CuM_2O_4 (M = Fe, Mn, Cr, Ga, Al and others) has greater stability than a commercial CuO–ZnO–Al_2O_3 metallic function [8–10,28]. It has also been proven that Ni addition attenuates Cu sintering, given that it improves surface dispersion and strengthens the interaction between Cu and γ-Al_2O_3 [26].

However, the use of γ-Al_2O_3 as an acid function for SRD has the additional inconvenience of promoting DME decomposition and the r-WGS reaction due to the high temperatures required for DME hydrolysis and, therefore, the formation of significant amounts of CH_4 and CO, which is a handicap for PEM fuel cells, given that CO concentrations lower than 50 ppm are required for avoiding anodic catalyst poisoning [29]. As an alternative to γ-Al_2O_3, acid functions of higher acidity have been proposed, such as 12-tungstosilicoheteropolyacids ($H_4SiW_{12}O_{40}$) deposited on γ-Al_2O_3 [30], WO_3/ZrO_2 [21,24,25], H-mordenite or HZSM-5 zeolites [5–7,20,22,23,31–33]. HZSM-5 zeolites are much more active for DME hydrolysis and allow obtaining high yields of H_2 at considerably lower temperatures (around 100 °C lower) than those required with γ-Al_2O_3 [5,6]. Nevertheless, due to their excessive acidity, they give way to hydrocarbons at temperatures close to 300 °C, which significantly reduces H_2 yield [7,31,32], and significant coking (deactivated catalyst) also occurs on the catalyst surface due to the condensation of the hydrocarbons formed [20]:

$$\text{Oxygenates} \rightarrow \text{hydrocarbons} \rightarrow \text{coke} \quad (6)$$

This paper studies the attenuation of HZSM-5 zeolite acidity by alkaline treatment (with NaOH) and the effect of treatment conditions on the physical–chemical properties of the zeolite. Likewise, the effect of this alkaline treatment is determined on the kinetic performance of: (i) the zeolite in DME hydrolysis (Eq. (2)) and (ii) the bifunctional catalyst (with CuO–ZnO–Al_2O_3 metallic function) prepared using different treated zeolites in the reforming of DME (Eq. (1)) and methanol (Eq. (3)), and in the formation of undesired byproducts, i.e., CO (Eq. (4)), CH_4 (Eq. (5)) and hydrocarbons (Eq. (6)). The study of coke deposition (second step in the scheme in Eq. (6)) is beyond the scope of this paper.

An alkaline treatment of the HZSM-5 zeolite is efficient for improving the kinetic behaviour and stability of the zeolite by attenuating acidity and mesopore generation. Accordingly, the condensation and coke formation reactions are attenuated in several processes, such as the transformation of methanol into olefins [34], the direct hydroxylation of benzene to phenol [35] and the selective transformation of aqueous ethanol into olefins [36,37].

2. Experimental

2.1. Catalyst synthesis

The bifunctional catalysts have been prepared by the wet physical mixing of CuO–ZnO–Al_2O_3 metallic function (called CZA, Cu/Zn/Al atomic ratio = 4.5:4.5:1.0), prepared by coprecipitating the corresponding nitrates with Na_2CO_3 at pH = 7.0 and 70 °C under conditions established in previous papers [38,39] and calcined at 325 °C for 3 h, and different acid functions, namely, γ-Al_2O_3, commercial HZSM-5 zeolite and HZSM-5 zeolites modified by different alkaline treatments. The homogeneous mixtures obtained are centrifuged to separate the solid, which is dried, firstly at ambient temperature for 24 h and then in an oven at 110 °C for another 24 h. The powder obtained is calcined at 325 °C for 3 h and subsequently pressed, ground and sieved to a particle size between 0.15 and 0.25 mm, which is suitable for a fluidized bed reactor. The content of the acid function is 85 wt% for the bifunctional catalyst with γ-Al_2O_3 and 50 wt% for the bifunctional catalysts with zeolite.

The alumina (supplied by *Derivados del Flúor* as $Al_2O_3{\cdot}H_2O$) has been calcined at 550 °C for 2 h in order to obtain the γ-Al_2O_3 phase, which has been denoted as ALU. The ZSM-5 zeolite (SiO_2/Al_2O_3 = 30) denoted as HZ30 has been supplied in ammonium form by *Zeolyst International*. The modified ZSM-5 zeolites have been obtained by alkaline treatment of the commercial zeolite. The alkaline treatment consists in ion exchanging the commercial ZSM-5 zeolite with NaOH solutions (*Panreac*, 99%) of different concentrations (0.2 or 0.4 M), by stirring at 80 °C for different times (10 or 300 min) and using a reflux condenser to prevent evaporation. The treated zeolites have been denoted A0.2-10, A0.2-300 and A0.4-300, where the first number refers to the molar concentration of the NaOH solution and the second number the duration (min) of the treatment.

The mixture is subsequently cooled rapidly in an ice bath, and the solid phase (separated by filtration using a paper of 0.8 μm pore size) is firstly dried for 24 h at room temperature and then at 110 °C for 24 h in an oven. The sodium zeolite is then exchanged with a 1 M solution of $NH_4(NO_3)$ (*Panreac*, 98%) at 80 °C for 2 h with constant stirring, whereupon the solid is separated by filtration, with this procedure being repeated twice. The resulting ammonium zeolite is washed twice (for 2 and 12 h by stirring with distilled water at room temperature) to remove the reagents, filtered and dried for 24 h at room temperature and then at 110 °C for another 24 h. The acid form of the parent zeolite and of the zeolites treated with NaOH have been obtained by calcination in a muffle furnace (*Thermicon P Heraeus, SA*) by carrying out the following sequences: ramp of 5 °C/min to 400 °C; 3 h at 400 °C; ramp of 3.3 °C/min to 450 °C; 16 h at 450 °C; ramp of 3.3 °C/min to 550 °C; 3 h at 550 °C and a cooling ramp of 4.4 °C/min to room temperature.

2.2. Catalyst characterization

The Si/Al ratio of the zeolites has been determined by X-ray fluorescence (XRF, *Philips MiniPal PW4025*). Crystallinity has been determined by X-ray diffraction (XRD, *Philips PW1710*) by applying the ASTM *Standards on Catalysis* [40] to the characteristic peaks of the HZSM-5 zeolite.

The porous structure has been determined by N_2 adsorption–desorption (*Micromeritics ASAP 2010*) and by Hg porosimetry (*Micromeritics Autopore 9220*). The metallic species liable to reduction and the temperature triggering the reduction have been determined by temperature programmed reduction (TPR, *AutoChem 2920 from Micromeritics*) by passing a 50 cm^3/min stream with 10% volume H_2 in Ar. The metal surface and the size of the metal crystallite (in the metallic function of the bifunctional catalysts) have been determined by chemisorption using N_2O pulses (*Micromeritics AutoChem 2920* coupled to a *Balzers Instruments Omnistar* mass spectrometer through a thermostated line in order to analyze the amounts both of N_2 formed and of unreacted N_2O by monitoring the signals corresponding to masses 28 and 44, respectively). Based on the volume of the gas reacted, the active surface of Cu has been calculated by considering the adsorbate surface area (1.63×10^{19} at Cu/m^2) and the adsorption stoichiometry (2 Cu atoms per oxygen atom) [41].

Total acidity and acid strength distribution have been measured by calorimetric measurements of the differential adsorption of ammonia and subsequent temperature programmed desorption (TPD) of NH_3, which have been carried out in a *Setaram TG-DSC 111* calorimeter connected on-line to a *Balzers Omnistar* mass spectrometer [42,43]. After de-gasing the zeolite sample (1 h in He stream at 500 °C), it has been cooled to 150 °C, and a syringe has been used to introduce an ammonia stream (10 μl/min) to saturate the sample, which has finally been swept with He at 150 °C to desorb physisorbed ammonia. The ratio between the continuous signals corresponding to heat flow and to weight change obtained during the ammonia adsorption step provides a measurement of the acid strength distribution, whereas the total amount of chemically retained base corresponds to the total acidity of the sample. Subsequently, the TPD of ammonia has been carried out by heating the sample at 5 °C/min to 550 °C, and the mass corresponding to desorbed ammonia has been registered in the mass spectrometer.

The nature of the sites (Brönsted or Lewis) has been determined by the FTIR spectroscopy of adsorbed pyridine (*Nicolet 6700* spectrometer provided with a *Specac* catalytic chamber). After subjecting the finely ground sample to a high vacuum at 400 °C for 30 min, temperature has been stabilized at 150 °C and successive pyridine pulses have been injected to saturate the sample, which has been subsequently subjected to a vacuum at 150 °C for 1 h to eliminate physisorbed pyridine, and the corresponding spectrum has been recorded. The Brönsted/Lewis ratio has been determined by integrating the bands at 1545 and 1450 cm^{-1} and taking into account the molar extinction coefficients of both adsorption bands [44].

2.3. Experimental set-up

The kinetic runs have been carried out in automated reaction equipment (*Microactivity Reference*, from *PID Eng & Tech*, Madrid, Spain) provided with a stainless steel isothermal fluidized-bed reactor of 22 mm internal diameter connected on-line to a *MicroGC Agilent 3000* for product analysis [39]. The hydrodynamic properties of the bed have been improved by mixing the catalyst (particle size between 0.15 and 0.25 mm) with inert alumina (particle size between 60 and 90 μm) in a catalyst/inert ratio of 1:4 in mass. The operating conditions are as follows: atmospheric pressure, steam/DME/He molar ratio = 3:1:0.85, temperature in the 225–325 °C range (300–400 °C for the ALU-based catalyst), space time up to 0.60 $g_{catalyst}$ h/g_{DME}, GHSV = 2100 h^{-1} (at 300 °C). Prior to the catalytic runs, the catalyst has been reduced using 10% H_2 in He at 300 °C for 2 h with a total flow rate of 60 ml/min.

2.4. Reaction indices

DME conversion, X_{DME}, and yield of H_2 and CO, Y_i, have been calculated as follows:

$$X_{DME} = \frac{F_{DME,0} - F_{DME}}{F_{DME,0}} \quad (7)$$

$$Y_i = \frac{F_i \cdot \upsilon_i^{-1}}{F_{DME,0}} \quad (8)$$

where F_i is the molar flow of i component at the reactor outlet, which is evaluated from its molar fraction (calculated from chromatographic results) and the total molar flow rate (determined by atomic balances for H, C and O), υ_i is the stoichiometric coefficient of i component produced in SRD (υ = 6 for H_2 and υ = 2 for CO and CO_2), and the subscript "0" denotes the inlet molar flow.

Furthermore, an additional reaction index is established, i.e., methanol effective conversion in the second step of the SRD process (Eq. (3)), X_{MeOH}:

$$X_{MeOH} = \frac{F_{MeOH,0} - F_{MeOH}}{F_{MeOH,0}} \quad (9)$$

where $F_{MeOH,0}$ is the methanol molar flow rate corresponding to DME conversion and is double the number of DME moles converted, according to the stoichiometry of DME hydrolysis (Eq. (2)).

Table 1
Physical and acid properties of commercial and synthesized acid functions.

Property	γ-Al_2O_3	HZ30	A0.2-10	A0.2-300	A0.4-300
Si/Al	0	15.3	14.1	13.0	10.5
S_{BET} (m^2/g)	186	484	496	466	395
$S_{external}$ (m^2/g)	184	170	172	176	175
$S_{micropore}$ (m^2/g)	2	314	324	290	221
$V_{micropore}$ (cm^3/g)	0	0.13	0.15	0.12	0.09
$V_{mesopore}$ (cm^3/g)	0.29	0.13	0.21	0.30	0.47
Total acidity (mmol NH_3/g)	0.05	0.90	0.75	0.71	0.67
Average acid strength (DSC) (kJ/mol NH_3)	105	130	125	120	110
Average acid strength (TPD), T_{max} (first peak) (°C)	330	246	247	263	264
Average acid strength (TPD), T_{max} (second peak) (°C)	–	420	414	409	400
Br/Lw ratio (150 °C)	0	4.1	3.5	2.8	2.2

3. Results and discussion

3.1. Effect of alkaline treatment on the properties of HZSM-5 zeolite

3.1.1. Effect on the porous structure

Table 1 shows the properties of the porous structure (determined by N_2 adsorption–desorption) and the Si/Al ratio (determined by XRF) of the acid functions. The Si/Al ratio of the commercial zeolite (HZ30) is consistent with the value given by the supplier and is lower in the zeolites treated with NaOH. The severity of the alkaline treatment significantly affects this ratio. Thus, it decreases as treatment time or NaOH concentration is increased. Furthermore, the treatment causes a significant decrease in zeolite mass (up to 30% under the more severe treatment, A0.4-300 zeolite), which is due to the partial dissolution of the zeolite by preferably extracting Si atoms from the structure [45–48].

Concerning physical properties, the lower BET surface area corresponds to γ-Al_2O_3 (a mesoporous material), with a narrow pore size distribution of around 33 Å (Fig. 1a).

A mild treatment with NaOH for 10 min (A0.2-10 zeolite) gives way to a significant increase in the mesopore volume of the zeolite, whereas the BET surface area and the micropore volume increase slightly because micropores of difficult access in the untreated zeolite (HZ30 zeolite) become accessible due to either mesopore formation [36] or the dissolution of amorphous Si species on the external surface, as has already been observed under mild treatments with NaOH [49]. However, as observed in Table 1 and Fig. 1a, increasing the severity of the alkaline treatment (A0.2-300 and A0.4-300 zeolites) leads to a lower surface area and micropore volume, whereas mesopore volume and mean pore diameter are higher. One explanation for this decrease in the volume of micropores lies in their partial blockage by the precipitation of an amorphous SiO_2 layer on the surface of HZSM-5 crystals, which is due to the formation of Si species dissolved during the alkaline treatment [47]. It should also be noted that the extraction of Si and Al atoms from the zeolite structure during the treatment may also cause micropore size enlargement, leading to the formation of mesopores [50].

Mesopore generation in the HZSM-5 zeolite by treating it with NaOH is well reported in the literature. Thus, the average mesopore size reported by certain authors is of around 40 Å [47,49], whereas others report a size of 100 Å [35,48]. The pore size distributions in Fig. 1b show the formation of mesopores of approximately 100 Å in the zeolite modified with the milder treatment (A0.2-10) and the moderate one (A0.2-300), with the mesopore volume being greater in the latter. Nevertheless, mesopores of around 250 Å are also formed in the zeolite modified with the most severe treatment (A0.4-300).

The SEM images for the original and modified zeolites (Fig. 2) do not reveal significant changes in their morphology, as was also observed by Bjorgen et al. [34] and Gopalakrishnan et al. [35], which explains why the external surface area of the zeolites does not change when treating them with NaOH (Table 1).

Although the zeolite does not maintain its BET surface area and mesopore distribution after the treatment with NaOH, the normalized XRD peaks (Fig. 3a) show that the crystal structure is maintained, given that no additional phases are observed. Nevertheless, relative crystallinity decreases subsequent to the treatment with NaOH due to either the preferential extraction of Si atoms from the structure [35,51] or the extraction of Al [47], without the crystalline structure being destroyed [52]. Relative crystallinity decreases by increasing both the treatment time and NaOH concentration.

3.1.2. Effect on acidity

Fig. 4a shows the acid strength distribution (heat released by mass unit of base adsorbed) and total acidity of the zeolites (HZ30 parent zeolite and that treated with NaOH). These results have

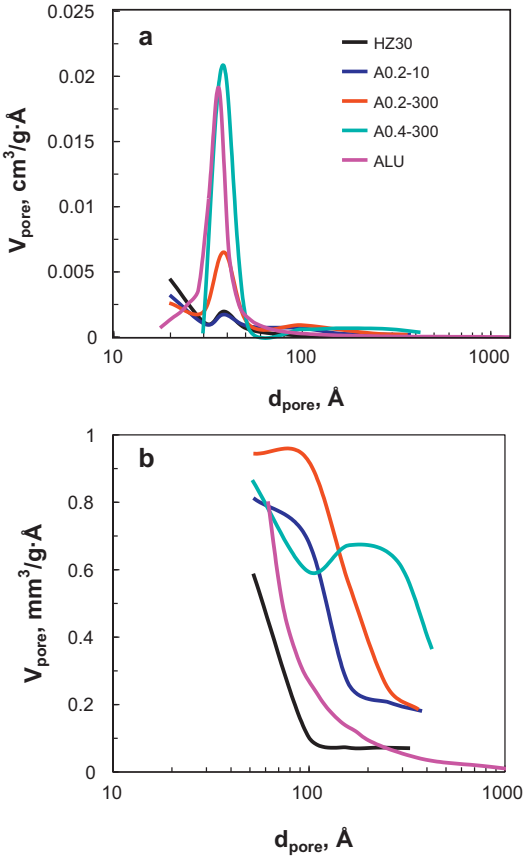

Fig. 1. Mesopore volume distribution of the acid functions (graph a) and enlarged 50–300 Å range (graph b).

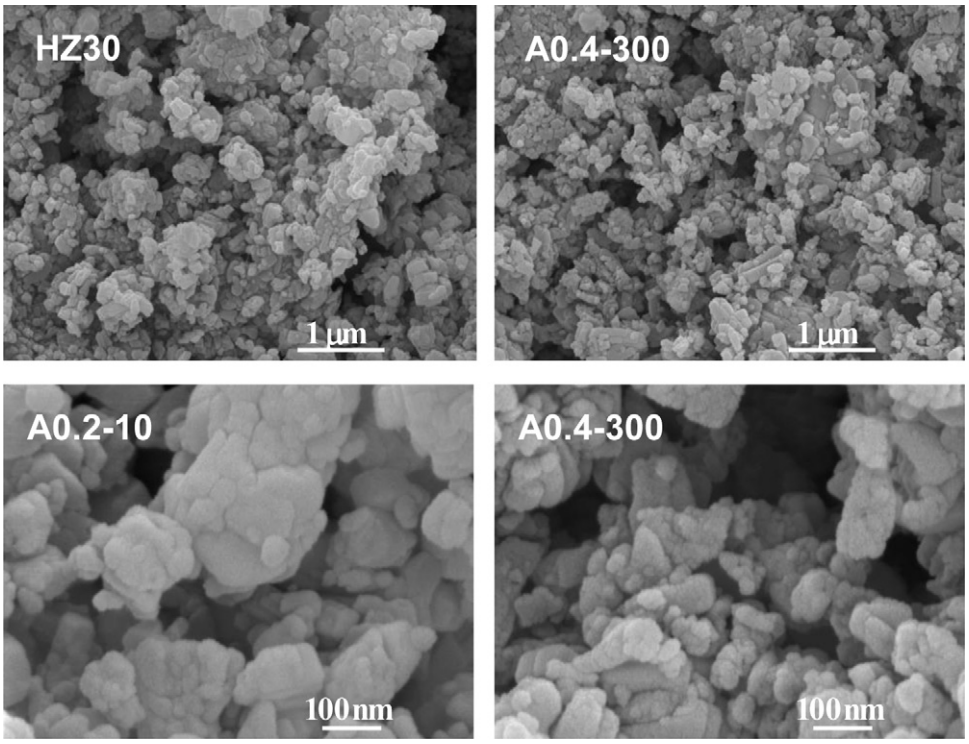

Fig. 2. SEM images of the parent zeolite (HZ30) and once it has undergone treatments of different severity with NaOH (A0.2-10 and A0.4-300).

been obtained in the differential adsorption of NH_3 at 150 °C, whereas Fig. 4b shows the corresponding results of temperature programmed desorption (TPD) of NH_3. The results for γ-Al_2O_3 have not been plotted because its acidity is approximately twenty times lower than that of HZ30 zeolite. Table 1 shows the acid properties (total acidity, average acid strength, temperature of the peaks in the TPD analysis, Brönsted/Lewis site ratio measured at 150 °C) for all the acid functions. As observed, γ-Al_2O_3 has a very low acidity, 0.05 mmol NH_3/g, and a moderate adsorption heat of around 105 kJ/mol NH_3.

The results in Table 1 show that the alkaline treatment causes a significant decrease in total acidity (from 0.90 mmol NH_3/g for the untreated HZ30 zeolite to 0.67 mmol NH_3/g for the one most severely treated with alkali, A0.4-300) and also affects the acid strength of the sites (which has a mean value of 130 kJ/mol NH_3 for the untreated zeolite, decreasing to 110 kJ/mol NH_3 for the most severely treated zeolite). Based on these results, the treatment with NaOH affects the total amount of sites to a greater extent than their acid strength, which is consistent with the results reported by Ogura et al. [47], Jia et al. [51] and Choi et al. [53].

The aforementioned results for total acidity and adsorption heat are similar to those reported in the literature for HZSM-5 zeolites with a Si/Al ratio in the 20–45 range, for which the total acidity values reported range from 0.41 to 0.70 mmol NH_3/g and average acid strength from 115 to 140 kJ/mol NH_3 [42,47,54,55]. For the HZSM-5 zeolite treated with NaOH, the values of total acidity reported range from 0.50 to 0.64 mmol NH_3/g and those of average acid strength from 100 to 130 kJ/mol NH_3 [36,47,48].

The TPD profiles of the HZSM-5 zeolites (Fig. 4b) reveal two types of sites of different strength: weak acid sites (desorption peak near 250 °C) and strong acid sites (desorption peak near 410 °C). The treatment with NaOH shifts the desorption peak corresponding to the strong acid sites to slightly lower temperatures. These results of NH_3 desorption are consistent with those obtained by DSC (Fig. 4a).

Fig. 5 shows the results corresponding to the amount of sites of different acid strength on the zeolites, which have been obtained through the deconvolution of TPD profiles (Fig. 4b) and integration in the ranges of 150–325 °C (weak sites) and 325–550 °C (strong sites). For the zeolites treated with NaOH, the amount of strong acid sites steadily decreases as the treatment is more severe, whereas the amount of weak acid sites remains almost constant.

Based on the aforementioned results, strong acid sites are the ones more affected by the alkaline treatment. Nevertheless, severe treatment with NaOH affects strong and weak sites alike, whereas a moderate treatment selectively attenuates the acidity of the strong acid sites, which is consistent with the results reported in the literature [47,51,52]. This may be explained by an increase in the relative concentration of Al with the alkaline treatment causing Al atoms to partially remain on the outside of the net, either as weak sites or even in an amorphous state, which is consistent with the XRD results [34,53].

The results in Table 1 allow concluding that γ-Al_2O_3 has only Lewis acidity and that the treatment of the zeolite with NaOH causes a decrease in the Br/Lw site ratio, more pronounced as the treatment is more severe, which evidences that Brönsted sites (strong sites) are selectively neutralized.

3.2. Effect of NaOH treatment on bifunctional catalyst properties

Table 2 shows the properties of the metallic function (which has been used with the different acid functions in the preparation of the catalysts by wet physical mixing of both functions) and the composition and physical–chemical properties of the bifunctional catalysts. It should be noted that the content of γ-Al_2O_3 in the CZA/ALU catalyst is 85 wt%, which is higher than that corresponding to the zeolites (50 wt%), given that the surface acidity of the γ-Al_2O_3 is lower and, consequently, higher amounts are required to obtain high values of conversion in DME reforming.

The wet physical mixing preserves the properties of each function and, consequently, the properties of the catalyst correspond to the theoretical values foreseen by the addition of both functions (±5% standard deviation). The properties of the

Table 2
Properties of CZA metallic function (CuO–ZnO–Al_2O_3, Cu/Zn/Al atomic ratio = 4.5:4.5:1.0), and of the bifunctional catalysts for SRD prepared by wet physical mixing of CZA metallic function and different acid functions.

Property	CZA	CZA/ALU	CZA/HZ30	CZA/A0.2-10	CZA/A0.2-300	CZA/A0.4-300
wt% metallic function (nominal)	–	15	50	50	50	50
wt% metallic function (real)	–	13.5	51.5	50.9	49.7	48.6
S_{BET} (m^2/g)	113	166	230	238	215	207
$V_{micropore}$ (cm^3/g)	–	–	0.06	0.06	0.05	0.04
$V_{mesopore}$ (cm^3/g)	0.49	0.28	0.18	0.20	0.27	0.33
d_{pore} (Å)	143	48	54	70	75	82
$S_{metallic}$ (m^2 Cu/g Cu)	141	19	56	62	70	56
$\bar{d}_{Cu}$ (Å)	48	364	120	108	96	119
Total acidity (mmol NH_3/g)	–	–	0.46	0.37	0.36	0.35
Average acid strength (kJ/mol NH_3)	–	–	125	120	115	103

bifunctional catalysts lie in the following ranges: BET surface area, 166–238 m^2/g; micropore volume, 0.04–0.06 cm^3/g; mesopore volume, 0.18–0.33 cm^3/g; mean diameter of Cu particles, 96–120 Å (for the bifunctional catalysts with the original HZSM-5 zeolite and once treated). The acid function has an essential impact on the physical properties and, especially, on acidity. Therefore, the effect of the alkaline treatment on catalyst properties is similar to that already noted for the acid function.

The specific metal surface area ($S_{metallic}$) of the catalyst is lower than that corresponding to the metallic function, which is due to the equilibration of the catalyst by calcination at 325 °C. Subsequent to this equilibration, the catalyst is slightly less active for SRD, but more stable because it does not undergo Cu sintering below 325 °C.

It is noted that the properties of the zeolite have no significant effect on the specific metal surface area and Cu average particle diameter (56–70 m^2 Cu/g Cu and 96–120 Å, respectively). Nevertheless, metal dispersion increases slightly when the zeolite is subjected to mild (A0.2-10) or moderate alkaline treatment (A0.2-300), but it decreases as the treatment is more severe (A0.4-300). A considerably lower specific metal surface area and a higher Cu crystal size in the bifunctional catalyst with γ-Al_2O_3 (CZA/ALU) explain the partial occlusion of the metallic function in a non-microporous acid function, which is the major component in the catalyst (85 wt%).

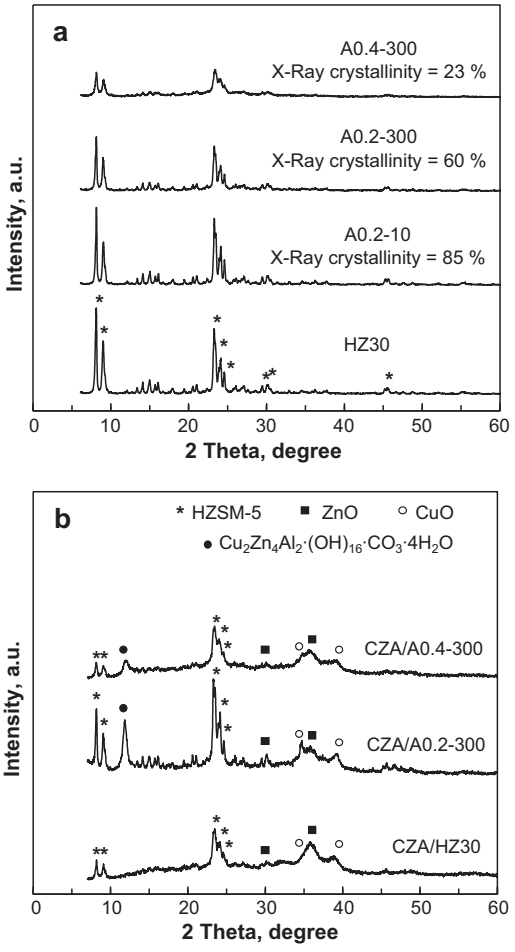

Fig. 3. X-ray diffractogram patterns of the parent zeolite (HZ30) and of the zeolites treated with NaOH (A0.2-10, A0.2-300, A0.4-300) (the characteristic peaks of HZSM-5 zeolites have been indicated) (graph a), and of the catalysts with CZA metallic function and different acid functions (graph b).

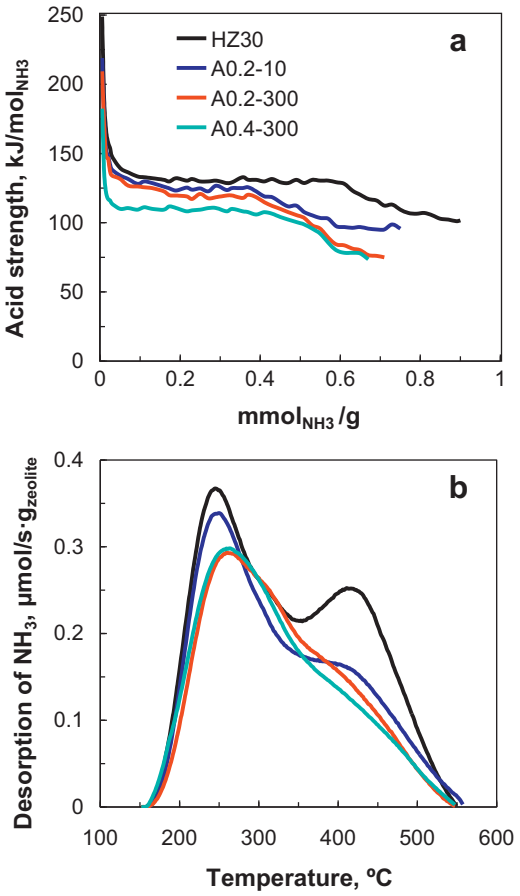

Fig. 4. Acid strength distribution (graph a) and TPD profiles of NH_3 (graph b), for the parent zeolite (HZ30) and for the zeolites treated with NaOH (A0.2-10, A0.2-300, A0.4-300).

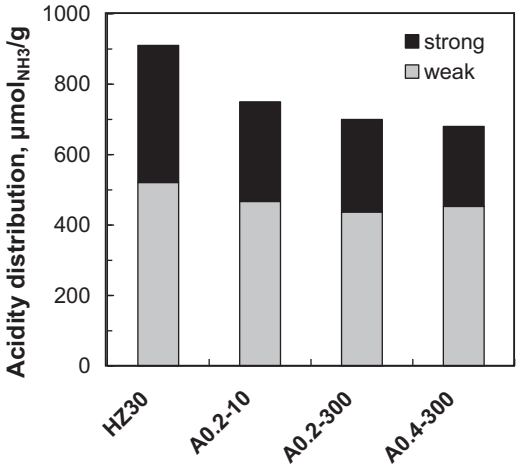

Fig. 5. Distribution of acid sites for the parent zeolite (HZ30) and for the zeolites treated with NaOH (A0.2-10, A0.2-300, A0.4-300).

XRD analysis (Fig. 3b) of the crystalline structure of the bifunctional catalysts shows the peaks corresponding to the individual phases of the bifunctional catalysts (CuO, ZnO, HZSM-5, γ-Al_2O_3).

Fig. 6 shows the temperature programmed reduction profiles (TPR) for the bifunctional catalysts. As observed, the acid function does not have a significant influence on the reducibility of the catalysts and, therefore, the TPR profiles are similar for all the catalysts, with a peak at around 175 °C corresponding to the reduction of Cu^{2+} phase [56], although this peak is shifted to a slightly higher temperature (190 °C) for the bifunctional catalysts with zeolite, either untreated or treated with alkali. The CZA/A0.2-300 bifunctional catalyst has a wider peak corresponding to higher metal-support interaction and higher metal dispersion. These results are consistent with the values of specific metal surface area shown in Table 2.

Fig. 7 shows the acid strength distribution of the bifunctional catalysts with the untreated zeolite (CZA/HZ30) and the zeolite subjected to severe alkaline treatment (CZA/A0.4-300). As observed, the total acidity of the catalyst is almost half that corresponding to the acid function, which is consistent with their content in the catalyst (50 wt%). Furthermore, as in the case of the zeolite, the alkaline treatment causes a more severe decrease in total acidity than in acid strength.

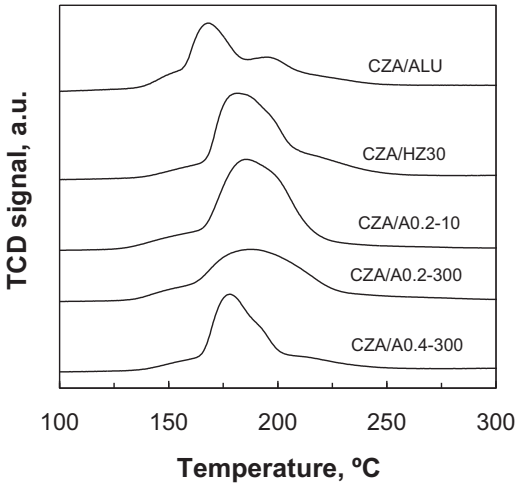

Fig. 6. TPR profiles for the catalysts with CZA metallic function and different acid functions.

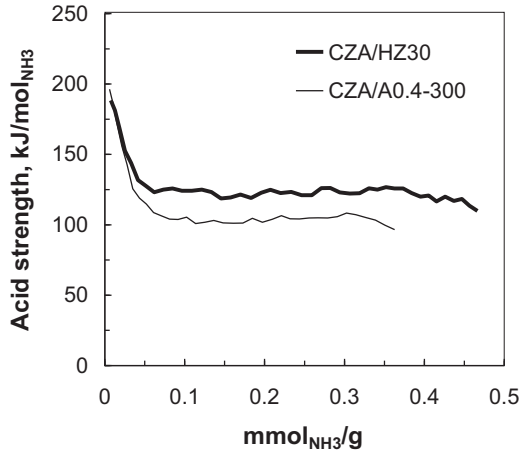

Fig. 7. Acid strength distribution for the CZA/HZ30 and CZA/A0.4-300 bifunctional catalysts.

3.3. Role of the acid function acidity in the DME hydrolysis step

Fig. 8 shows the temperature effect the different acid functions have on DME conversion (Fig. 8a) and hydrocarbon molar fraction (Fig. 8b), which are secondary products at the reactor outlet. The major component is methanol because the main reaction is DME hydrolysis (Eq. (2)). The reactions have been carried out with the

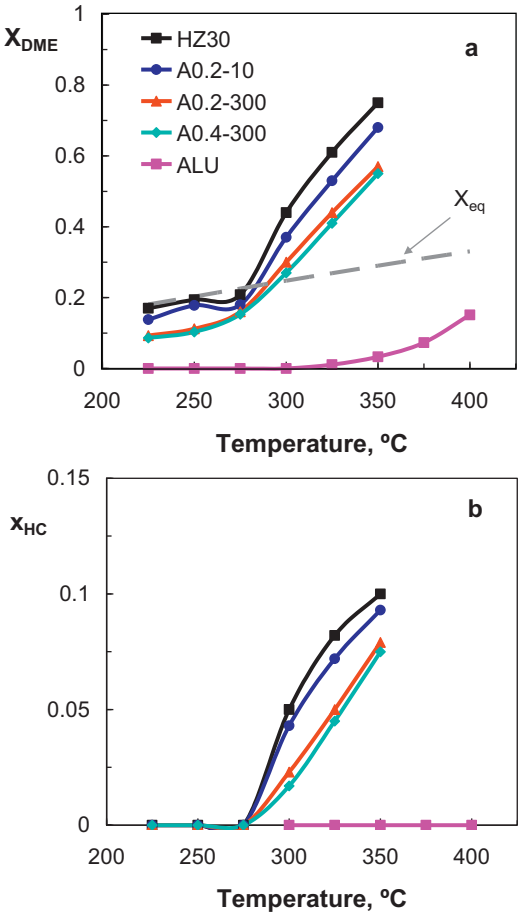

Fig. 8. Effect of temperature on DME conversion (graph a) and hydrocarbon molar fraction (graph b) at zero time on stream, for the different acid functions. Reaction conditions: 1.2 bar, steam/DME molar ratio = 3:1, space time = 0.15 $g_{catalyst}$ h/g_{DME}, and P_{DME} = 0.21 bar.

same steam/DME molar ratio in the feed (steam/DME = 3:1) as in the DME reforming runs. The results correspond to zero time on stream, and the formation of secondary hydrocarbons (according to the reaction in Eq. (6)) is an undesired result, with its minimization conditioning the selection of the acid function. DME transformation by hydrolysis (Eq. (2)) and hydrocarbon formation (Eq. (6)) are parallel reactions, whose relative importance depends on the reaction conditions. Fig. 8a also shows the increase in the equilibrium conversion for DME hydrolysis reaction (Eq. (2)) as temperature is increased, which is due to the endothermic nature of hydrolysis.

It should be noted that the results shown in Fig. 8 have been obtained with a low space time (0.15 $g_{catalyst}$ h/g_{DME}), which allows comparing the catalysts when product formation is incipient. Under these conditions, higher activity is observed for the HZSM-5 zeolite than for γ-Al_2O_3 in DME hydrolysis (Fig. 8a), and the activity of the latter is insignificant for the formation of hydrocarbons (Fig. 8b). Under the conditions used, a significant conversion of DME with γ-Al_2O_3 is reached only above 350 °C, and the formation of CH_4 (Eq. (5)) and hydrocarbons (Eq. (6)) is insignificant in the temperature range studied. The formation of CH_4 reported in the literature by other authors is explained by differences in reaction conditions enhancing the thermal decomposition of DME [6,19].

The results in Fig. 8 show a higher reaction rate for hydrolysis than hydrocarbon formation (although this is only significant above 275 °C). The conversion in DME hydrolysis is higher than 0.1 for all the zeolites above 225 °C (Fig. 8a). Furthermore, the formation of hydrocarbons is significant above 300 °C for all the zeolites (Fig. 8b). These hydrocarbons are C_2—C_4 compounds, with ethylene being the main component.

The significance of the alkaline treatment is also noteworthy. As the severity of the treatment is increased, DME conversion decreases for the same temperature (Fig. 8a), but the formation of hydrocarbons is also attenuated (Fig. 8b). This effect is a consequence of the different acid properties of the zeolites (Table 1). Higher acidity enhances DME hydrolysis and hydrocarbon formation, and both reactions are attenuated as the alkaline treatment is more severe.

In view of these results, it should be noted that HZSM-5 zeolites allow carrying out DME hydrolysis at lower temperatures than γ-Al_2O_3, with the resulting energy saving, which is essential for process viability. Furthermore, their use in a bifunctional catalyst together with a Cu metallic function requires an acid function with high activity for DME hydrolysis at 300 °C in order to avoid irreversible deactivation by Cu sintering. Furthermore, regarding the attenuation of the undesired formation of hydrocarbons (significant above 300 °C), the results in Fig. 8 show that the alkaline treatment applied to the zeolite is efficient.

The transformation of DME into hydrocarbons on a HZSM-5 zeolite is a well-known reaction because it is an essential step in the transformation of methanol into hydrocarbons (MTH process) [57], in which the DME formation rate is very fast and is almost in equilibrium with methanol. DME is also known for its higher reactivity for hydrocarbon formation than methanol [58]. The mechanism involving the transformation of oxygenates (methanol/DME) into hydrocarbons on a HZSM-5 zeolite has been widely studied in the literature, given that it is extremely relevant for the selective production of gasoline pool C_5—C_{11} hydrocarbons (MTG process) and C_2—C_4 olefins (primary products) through the MTO process. The suitable performance of HZSM-5 is a consequence of its moderate acid levels and shape selectivity, which are appropriate for minimizing the secondary reactions (mainly hydrogen transfer) forming aromatics and the coke that causes pore blockage [59].

The generally accepted mechanism (hydrocarbon pool mechanism) for the first step in the transformation of methanol/DME into hydrocarbons considers the formation of methylbenzenes and cyclopentyl cations as intermediates that release C_2—C_4 olefins as primary products [34,60,61]. These olefins are subsequently transformed into higher hydrocarbons by oligomerization-cracking, isomerization, alkylation, cyclization and the condensation to aromatics [62,63]. It has been well reported that a reduction in the acid strength of the HZSM-5 sites attenuates the rates of the steps of olefin formation and subsequent hydrocarbon transformation [43,64]. Consequently, the coke precursor condensation steps are also attenuated, and therefore deactivation is minimized [65,66].

A feature of the hydrocarbon pool mechanism is the need for an induction period for the formation of reaction intermediates, with the hydrocarbon formation rate being significant after this period. The length of this period depends on the properties of the catalyst (decreasing as the acidity of the HZSM-5 zeolite is increased) and reaction conditions, i.e., decreasing as temperature is raised and increasing as the steam content in the reaction medium rises [67–69].

3.4. Role of bifunctional catalyst acidity in DME reforming

Fig. 9 shows the effect of temperature on DME conversion at zero time on stream (Eq. (7)) (Fig. 9a), methanol effective conversion (Eq. (9)) (Fig. 9b) and yields (Eq. (8)) of H_2 (Fig. 9c) and CO (Fig. 9d), for the bifunctional catalysts prepared using the different acid functions. These results have been obtained in short runs (30 min) carried out under the following conditions: temperature, 225, 250, 275, 300 and 325 °C with the zeolite based bifunctional catalysts, and 300, 325, 350, 375 and 400 °C with the γ-Al_2O_3 based bifunctional catalyst; pressure, 1.2 bar; steam/DME molar ratio, 3:1; space time, 0.60 $g_{catalyst}$ h/g_{DME}; partial pressure of DME (diluted with He), 0.21 bar. The ceiling temperature for the experiments using zeolite based bifunctional catalysts has been set at 325 °C to avoid Cu sintering, whereas operation has been carried out at higher temperatures with the γ-Al_2O_3 based bifunctional catalyst in order to attain significant H_2 yields. Furthermore, CH_4 formation by DME decomposition is insignificant even at 400 °C.

An increase in temperature enhances DME reforming, given that the conversions of DME (Fig. 9a) and methanol (Fig. 9b) are increased and, therefore, the yield of H_2 (Fig. 9c) is higher. Nevertheless, an increase in temperature also increases the yield of CO (Fig. 9d) due to the enhancement of r-WGS reaction thermodynamics (Eq. (4)).

The results for SRD are consistent with those noted earlier for DME hydrolysis (Fig. 8). Given the significance of acid function acidity in the reforming rate-limiting step, which is DME hydrolysis, the catalyst order for DME conversion (Fig. 9a) and H_2 yield (Fig. 9c) is the same as the order for total acidity and acid strength (Table 2).

CZA/HZ30 > CZA/A0.2-10 > CZA/A0.2-300 > CZA/A0.4-300

Nevertheless, this order is the same as for CO formation by r-WGS reaction (Fig. 9d), which is also enhanced by the higher concentrations of H_2 and CO_2 available in the reaction medium when more acid catalysts are used. Methanol reforming occurs on the metallic function and, therefore, methanol effective conversion (Fig. 9b) is almost independent of the acid function.

3.5. Hydrocarbon formation and stability of bifunctional catalysts

Fig. 10 shows the evolution with time on stream for DME conversion (Fig. 10a) and molar fractions at the reactor outlet for methanol (Fig. 10b), H_2 (Fig. 10c) and hydrocarbons (Fig. 10d). Runs of 550 min have been carried out by following increasing temperature steps, with a constant temperature for 1–2 h in each step, and a heating ramp of 5 °C/min between steps. The remaining conditions are the same as those in Fig. 9. In view of their interest (high conversion), the steps corresponding to 275, 300 and 325 °C are shown.

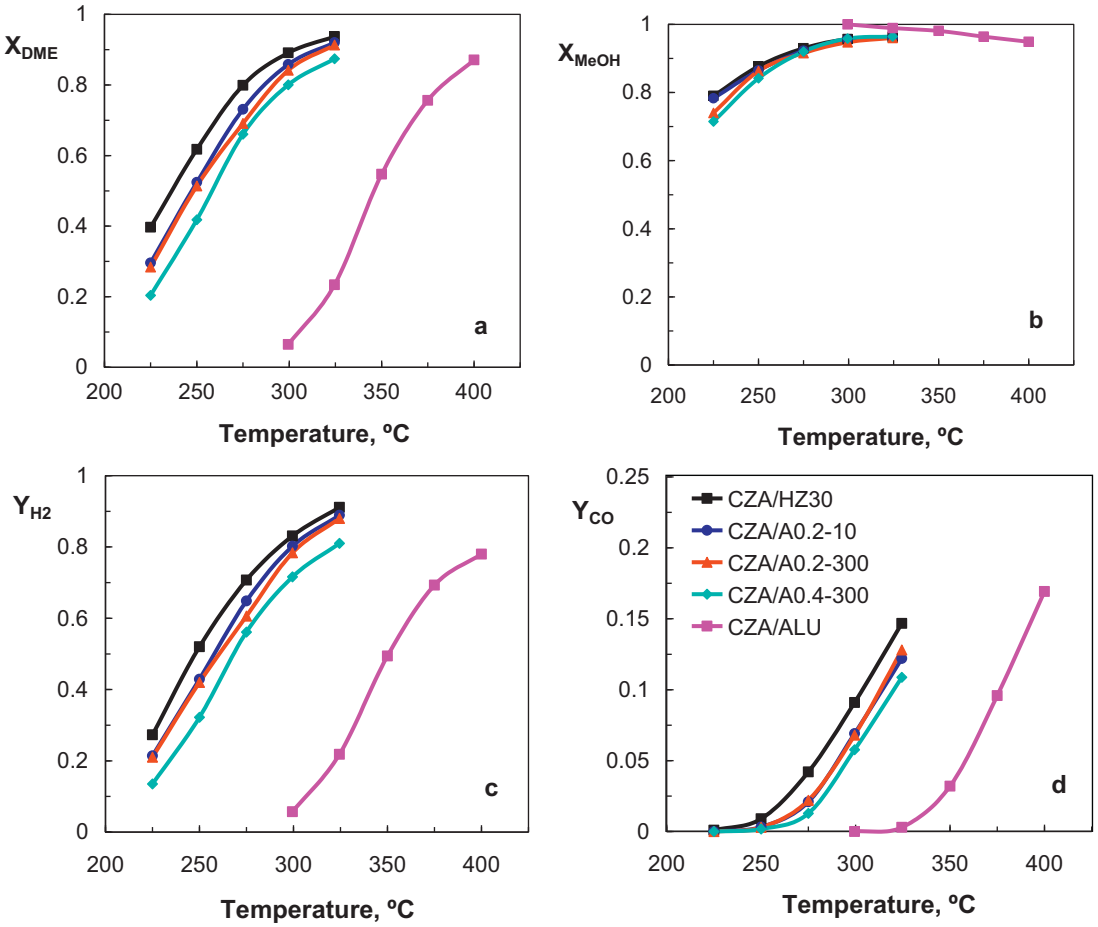

Fig. 9. Effect of temperature on DME conversion (graph a), methanol effective conversion (graph b), H_2 yield (graph c) and CO yield (graph d) at zero time on stream, for the catalysts with CZA metallic function and different acid functions. Reaction conditions: 1.2 bar, steam/DME molar ratio = 3:1, space time = 0.60 $g_{catalyst}$ h/g_{DME}, and P_{DME} = 0.21 bar.

The results at 300 °C show that DME conversion (Fig. 10a) and H_2 molar fraction (Fig. 10c) decrease slightly with time on stream when the bifunctional catalyst prepared with the parent zeolite (CZA/HZ30) is used, whereas the methanol molar fraction (Fig. 10b) increases slightly. Nevertheless, these reaction indices remain constant when the catalysts prepared with the zeolites treated with NaOH are used. This different stability of the catalysts is associated with the formation of hydrocarbons (Fig. 10d), which is incipient at 300 °C for the catalyst prepared with the parent zeolite and is not significant for the catalysts prepared with the treated zeolites. It should be noted that the yield of hydrocarbons at 300 °C is significant when the acid function is used (Fig. 8b), and the attenuation of their formation when bifunctional catalysts are used (Fig. 10d) is explained by the increase in the DME hydrolysis reaction rate due to the shift of the thermodynamic equilibrium by methanol reforming.

The formation of hydrocarbons at 325 °C is significant for all the bifunctional catalysts except for the one prepared with the zeolite subjected to the most severe alkaline treatment (CZA/A0.4-300), for which the formation of hydrocarbons is insignificant (Fig. 10d). This catalyst is stable and the indices remain constant with time on stream for DME conversion (Fig. 10a) and reactor outlet concentrations of methanol (Fig. 10b) and H_2 (Fig. 10c).

The relationship between hydrocarbon formation and catalyst stability is explained by the competition between the hydrocarbon formation reaction (Eq. (6)) and DME reforming steps (Eqs. (2) and (3)), given that C_2–C_4 hydrocarbon molecules are adsorbed on the metallic sites of the catalysts by competing with methanol and, therefore, attenuating its reforming (Eq. (3)). Consequently, H_2 concentration decreases in the reaction medium, but increases for methanol. The increase in the concentration of methanol shifts the hydrolysis reaction equilibrium (Eq. (2)) and, therefore, DME conversion decreases.

The stability of the catalysts has been studied by carrying out long runs (12 h) at 300 °C—a temperature at which the formation of hydrocarbons is appreciated only with the catalyst prepared with the parent zeolite (CZA/HZ30). The catalyst prepared with γ–Al_2O_3 (CZA/ALU) has been used at 400 °C for a significant H_2 yield. Regarding this catalyst, Cu average particle size increases significantly, from 364 Å for the fresh catalyst to 840 Å for the catalyst used for 12 h at 400 °C. Cu average particle size remains constant for the zeolite based bifunctional catalysts used below 325 °C.

Fig. 11 shows the evolution of H_2 yield with time on stream for the different catalysts. The H_2 yield with CZA/ALU catalyst decreases from 70% at zero time on stream to 35% (a value reached approximately in 12 h), which is attributed to the aforementioned Cu sintering at 400 °C. Consequently, an equilibration of this catalyst by long calcination at 400 °C would render it stable for SRD, but with very low activity compared to the catalysts prepared using HZSM-5 zeolites.

The catalyst prepared with the parent zeolite (CZA/HZ30) is stable for 10 h and, subsequently, the yield of H_2 decreases sharply. This decrease in reforming activity is associated with hydrocarbon formation, which is incipient, but has already been appreciated in Fig. 10d when this catalyst is used at 300 °C. The physical properties of CZA/HZ30 bifunctional catalyst are considerably deteriorated

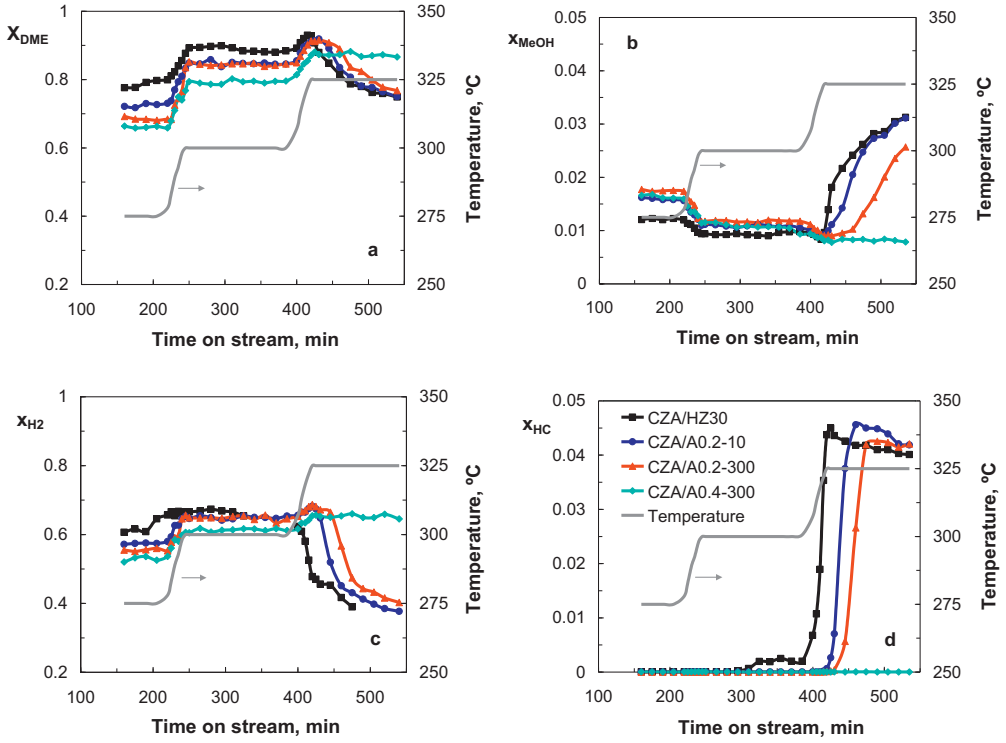

Fig. 10. Evolution with time on stream of DME conversion (graph a) and molar fractions of methanol (graph b), H_2 (graph c) and hydrocarbons (graph d) in the runs with increasing temperature steps for the catalysts with CZA metallic function and different acid functions. Reaction conditions: 1.2 bar, steam/DME molar ratio = 3:1, space time = 0.60 $g_{catalyst}$ h/g_{DME}, and P_{DME} = 0.21 bar.

subsequent to the reaction. Its BET surface area decreases from 230 m^2/g for the fresh catalyst (Table 2) to 156 m^2/g once it has been used under the conditions shown in Fig. 11. Micropore volume also decreases considerably (from 0.06 cm^3/g at zero time on stream to 0.03 cm^3/g) and pore diameter increases significantly (from 54 Å to 95 Å). The values of the physical properties for the used CZA/HZ30 catalyst are consistent with the sharp decrease in the H_2 production observed in the final reaction stages (Fig. 11), which evidences that a fraction of the micropores has been blocked. A significant deterioration is also observed in the metallic properties for CZA/HZ30 catalyst, i.e., the specific metal surface area decreases (from 56 m^2 Cu/g Cu for the fresh catalyst to 40 m^2 Cu/g Cu for the used catalyst) and the average Cu particle size increases (from 120 Å to 160 Å). Based on these results, coke deposition is probably the cause of catalyst deactivation, as has been observed by other authors in bifunctional catalysts of similar composition [70,71].

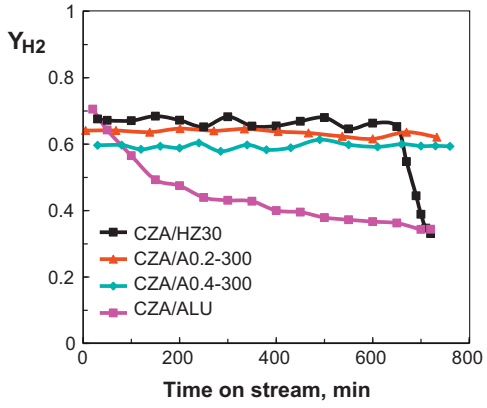

Fig. 11. Evolution of H_2 yield with time on stream for the catalyst with CZA metallic function and different acid functions. Reaction conditions: 300 °C for the zeolite based bifunctional catalysts, and 400 °C for the γ-Al_2O_3 based bifunctional catalyst, 1.2 bar, steam/DME molar ratio = 3:1, space time = 0.25 $g_{catalyst}$ h/g_{DME}, GHSV = 5000 h^{-1}, and P_{DME} = 0.21 bar.

The catalysts prepared using NaOH treated zeolites (CZA/A0.2-300 and CZA/A0.4-300) are stable for the time on stream studied. In contrast to CZA/HZ30 catalyst, the physical and metallic properties of CZA/A0.4-300 catalyst hardly change subsequent to reaction under the conditions in Fig. 11. The BET surface area for CZA/A0.4-300 catalyst remains almost constant (207 m^2/g for the fresh catalyst, Table 2, and 202 m^2/g for the used one), while the specific metal surface area decreases slightly (from 56 m^2 Cu/g Cu to 52 m^2 Cu/g Cu) and the average Cu particle size increases very slightly (from 119 Å to 126 Å). Nevertheless, the study has been conducted with low values of space time for comparing catalysts and monitoring their deactivation. Runs would be interesting with higher space time values (almost full DME conversion) and for a long time in order to assess the industrial applicability of these catalysts, particularly that prepared using the zeolite subjected to the most severe treatment (CZA/A0.4-300), for which H_2 yield remains constant for 60 h.

4. Conclusions

The bifunctional catalyst prepared by wet physical mixing of CuO–ZnO–Al_2O_3 (Cu/Zn/Al atomic ratio = 4.5:4.5:1.0, prepared by co-precipitation) and HZSM-5 zeolite, with both functions at 50 wt%, is much more active for DME reforming than the catalyst prepared using γ-Al_2O_3 acid function, whereby the reaction can be conducted at much lower temperatures, thus saving energy and also avoiding Cu sintering. Nevertheless, C_2—C_4 hydrocarbons are formed due to the HZSM-5 zeolite's high acidity and acid strength values. This hydrocarbon formation reduces the catalyst's reforming capacity presumably due to the competitive adsorption of hydrocarbons and methanol on the metallic function.

The alkaline treatment of the HZSM-5 zeolite is efficient for decreasing total acidity and attenuating the acid strength of the zeolite. This treatment slightly decreases zeolite activity in the DME hydrolysis step, and has a major effect on the formation of hydrocarbons in DME reforming, i.e., as the alkaline treatment is more severe, higher temperatures are required for hydrocarbon formation.

Severe alkaline treatment (with 0.4 M NaOH solution for 300 min) is suitable for modifying the HZSM-5 zeolite in order to use it as an acid function for DME steam reforming with $CuO–ZnO–Al_2O_3$ as metallic function. This alkaline treatment moderates the acidity of the zeolite, thereby avoiding the formation of hydrocarbons at 300 °C and minimizing the formation of CO and deactivation by Cu sintering. Although acidity is attenuated, the catalyst remains active for DME reforming with high H_2 yield and selectivity. The catalyst is stable at 300 °C and its kinetic behaviour remains constant with time on stream.

Acknowledgements

This work has been carried out with financial support from the Ministry of Science and Technology of the Spanish Government (Projects CTQ2006-12006 and CTQ2009-13428), the University of the Basque Country (UFI 11/39) and the Basque Government (Project GIC07/24-IT-220-07).

References

[1] S. Hočevar, W. Summers, Hydrogen production, in: A. León (Ed.), Hydrogen Technology, Springer-Verlag, Berlin/Heidelberg, 2008, pp. 15–79.
[2] M. Balat, International Journal of Hydrogen Energy 33 (2008) 4013–4029.
[3] S. Sá, H. Silva, L. Brandão, J.M. Sousa, A. Mendes, Applied Catalysis B 99 (2010) 43–57.
[4] Y. Tanaka, R. Kikuchi, T. Takeguchi, K. Eguchi, Applied Catalysis B 57 (2005) 211–222.
[5] T.A. Semelsberger, K.C. Ott, R.L. Borup, H.L. Greene, Applied Catalysis A 309 (2006) 210–223.
[6] T.A. Semelsberger, K.C. Ott, R.L. Borup, H.L. Greene, Applied Catalysis B 65 (2006) 291–300.
[7] K. Faungnawakij, R. Kikuchi, T. Matsui, T. Fukunaga, K. Eguchi, Applied Catalysis A 333 (2007) 114–121.
[8] K. Faungnawakij, Y. Tanaka, N. Shimoda, T. Fukunaga, R. Kikuchi, K. Eguchi, Applied Catalysis B 74 (2007) 144–151.
[9] K. Faungnawakij, N. Shimoda, T. Fukunaga, R. Kikuchi, K. Eguchi, Applied Catalysis A 341 (2008) 139–145.
[10] K. Faungnawakij, T. Fukunaga, R. Kikuchi, K. Eguchi, Journal of Catalysis 256 (2008) 37–44.
[11] T. Fukunaga, N. Ryumon, S. Shimazu, Applied Catalysis A 348 (2008) 193–200.
[12] T.A. Semelsberger, R.L. Borup, H.L. Greene, Applied Catalysis A 156 (2006) 497–511.
[13] A.T. Aguayo, J. Ereña, I. Sierra, M. Olazar, J. Bilbao, Catalysis Today 106 (2005) 265–270.
[14] A.T. Aguayo, J. Ereña, D. Mier, J.M. Arandes, M. Olazar, J. Bilbao, Industrial & Engineering Chemistry Research 46 (2007) 5522–5530.
[15] J. Ereña, I. Sierra, A.T. Aguayo, A. Ateka, M. Olazar, J. Bilbao, Chemical Engineering Journal 174 (2011) 660–667.
[16] G.A. Olah, A. Goeppert, G.K.S. Prakash, Journal of Organic Chemistry 74 (2009) 487–498.
[17] S.D. Badmaev, P.V. Snytnikov, International Journal of Hydrogen Energy 33 (2008) 3026–3030.
[18] K. Takeishi, H. Suzuki, Applied Catalysis A 260 (2004) 111–117.
[19] T.A. Semelsberger, K.C. Ott, R.L. Borup, H.L. Greene, Applied Catalysis A 61 (2005) 281–287.
[20] T. Kawabata, H. Matsuoka, T. Shisido, D. Li, Y. Tian, T. Sano, K. Takehira, Applied Catalysis A 308 (2006) 82–90.
[21] S.D. Badmaev, G.G. Volkova, V.D. Belyaev, V.A. Sobyanin, Reaction Kinetics and Catalysis Letters 90 (2007) 205–211.
[22] D. Feng, Y. Zuo, D. Wang, J. Wang, Chinese Journal of Catalysis 30 (2009) 223–229.
[23] T. Matsumoto, T. Nishiguchi, H. Kanai, K. Utani, Y. Matsumura, S. Imamura, Applied Catalysis A 276 (2004) 267–273.
[24] T. Nishiguchi, K. Oka, T. Matsumoto, H. Kanai, K. Utani, S. Imamura, Applied Catalysis A 301 (2006) 66–74.
[25] K. Oka, T. Nishiguchi, H. Kanai, K. Utani, S. Imamura, Applied Catalysis A 309 (2006) 187–191.
[26] X. Wang, X. Pan, R. Lin, S. Kou, W. Zou, J.X. Ma, International Journal of Hydrogen Energy 35 (2010) 4060–4068.
[27] Y. Yamada, T. Mathew, A. Ueda, H. Shioyama, T. Kobayashi, Applied Surface Science 252 (2006) 2593–2597.
[28] K. Faungnawakij, N. Shimoda, N. Viriya-Empikul, R. Kikuchi, K. Eguchi, Applied Catalysis B 97 (2010) 21–27.
[29] J. Xuan, M.K.H. Leung, D.Y.C. Leug, M. Ni, Renewable & Sustainable Energy Reviews 13 (2009) 1301–1313.
[30] V.V. Galvita, G.L. Semin, V.D. Belyaev, T.M. Yurieva, V.A. Sobyanin, Applied Catalysis A 216 (2001) 85–90.
[31] K. Faungnawakij, Y. Tanaka, N. Shimoda, T. Fukunaga, S. Kawashima, R. Kikuchi, K. Eguchi, Applied Catalysis A 304 (2006) 40–48.
[32] N. Shimoda, K. Faungnawakij, R. Kikuchi, K. Eguchi, Applied Catalysis A 378 (2010) 234–242.
[33] N. Shimoda, K. Faungnawakij, R. Kikuchi, K. Eguchi, International Journal of Hydrogen Energy 36 (2011) 1433–1441.
[34] M. Bjorgen, F. Joensen, M. Spangsberg Holm, U. Olsbye, K.P. Lillerud, S. Svelle, Applied Catalysis A 345 (2008) 43–50.
[35] S. Gopalakrishnan, A. Zampieri, W. Schwieger, Journal of Catalysis 260 (2008) 193–197.
[36] A.G. Gayubo, A. Alonso, B. Valle, A.T. Aguayo, J. Bilbao, Applied Catalysis B 97 (2010) 299–306.
[37] A.G. Gayubo, A. Alonso, B. Valle, A.T. Aguayo, J. Bilbao, Industrial & Engineering Chemistry Research 49 (2010) 10836–10844.
[38] J. Ereña, J.M. Arandes, R. Garoña, A.G. Gayubo, J. Bilbao, Journal of Chemical Technology & Biotechnology 78 (2003) 161–166.
[39] J. Ereña, J. Vicente, A.T. Aguayo, A.G. Gayubo, M. Olazar, J. Bilbao, Applied Catalysis A, submitted for publication.
[40] A. Jentys, J.A. Lercher, Introduction to Zeolite Science and Practice, 2nd edition, Elsevier, Amsterdam, 2001.
[41] J.W. Evans, M.S. Wainwright, A.J. Bridgewater, D.J. Young, Applied Catalysis 7 (1983) 75–83.
[42] A.G. Gayubo, P.L. Benito, A.T. Aguayo, M. Olazar, J. Bilbao, Journal of Chemical Technology & Biotechnology 65 (1996) 186–192.
[43] A.T. Aguayo, A.G. Gayubo, R. Vivanco, M. Olazar, J. Bilbao, Applied Catalysis A 283 (2005) 197–207.
[44] C.A. Emeis, Journal of Catalysis 141 (1993) 347–354.
[45] R.M. Dessau, E.W. Valyocsik, N.H. Goeke, Zeolites 12 (1992) 776–779.
[46] A. Cizmek, B. Subotic, R. Aiello, F. Crea, A. Nastro, C. Tuoto, Microporous Materials 4 (1995) 159–168.
[47] M. Ogura, S.Y. Shinomiya, J. Tateno, Y. Nara, M. Nomura, E. Kikuchi, M. Matsukata, Applied Catalysis A 219 (2001) 33–43.
[48] Y. Li, S. Liu, S. Xie, L. Xu, Applied Catalysis A 360 (2009) 8–16.
[49] Y.Q. Song, Y.L. Feng, F. Liu, C.L. Kang, X.L. Zhou, L.Y. Xu, G.X. Yu, Journal of Molecular Catalysis A 310 (2009) 130–137.
[50] J.S. Jung, J.W. Park, G. Seo, Applied Catalysis A 288 (2005) 149–157.
[51] A. Jia, L.L. Lou, C. Zhang, Y. Zhang, S. Liu, Journal of Molecular Catalysis A 306 (2009) 123–129.
[52] J.C. Groen, L.A.A. Peffer, J.A. Moulijn, J. Peréz-Ramírez, Colloids and Surfaces A 241 (2004) 53–58.
[53] D.H. Choi, J.W. Park, J.H. Kim, Y. Sugi, G. Seo, Polymer Degradation and Stability 91 (2006) 2860–2866.
[54] B. Dragoi, A. Gervasini, E. Dumitriu, A. Auroux, Thermochimica Acta 420 (2004) 127–134.
[55] K. Suzuki, Y. Aoyagi, N. Katada, M. Choi, R. Ryoo, M. Niwa, Catalysis Today 132 (2008) 38–45.
[56] J. Agrell, M. Boutonnet, I. Melián-Cabrera, J.L.G. Fierro, Applied Catalysis A 253 (2003) 201–211.
[57] M. Stöcker, Microporous and Mesoporous Materials 29 (1999) 3–48.
[58] A.G. Gayubo, A.T. Aguayo, M. Olazar, R. Vivanco, J. Bilbao, Chemical Engineering Science 58 (2003) 5239–5249.
[59] M. Guisnet, L. Costa, F. Ramôa Ribeiro, Journal of Molecular Catalysis A 305 (2009) 69–83.
[60] J.F. Haw, J.B. Nicholas, W. Song, F. Deng, Z. Wang, T. Xu, C.S. Heneghan, Journal of American Chemical Society 122 (2000) 4763–4775.
[61] S. Svelle, F. Joensen, J. Nerlov, U. Olsbye, K.P. Lillerud, S. Kolboe, M. Bjørgen, Journal of American Chemical Society 128 (2006) 14770–14771.
[62] A.T. Aguayo, D. Mier, A.G. Gayubo, M. Gamero, J. Bilbao, Industrial & Engineering Chemistry Research 49 (2010) 12371–12378.
[63] M. Kaarsholm, B. Rafii, F. Joensen, R. Cenni, J. Chaouki, G.S. Patience, Industrial & Engineering Chemistry Research 49 (2010) 29–38.
[64] Y. Yang, C. Sun, J. Du, Y. Yue, W. Hua, C. Zhang, W. Shen, H. Xu, Catalysis Communications 24 (2012) 44–47.
[65] A.T. Aguayo, P.L. Benito, A.G. Gayubo, M. Olazar, J. Bilbao, Studies in Surface Science and Catalysis 88 (1994) 567–572.
[66] P.L. Benito, A.G. Gayubo, A.T. Aguayo, M. Castilla, J. Bilbao, Industrial & Engineering Chemistry Research 35 (1996) 81–89.
[67] A.T. Aguayo, A.G. Gayubo, R. Vivanco, A. Alonso, J. Bilbao, Industrial & Engineering Chemistry Research 44 (2005) 7279–7286.
[68] A.G. Gayubo, R. Vivanco, A. Alonso, B. Valle, A.T. Aguayo, Industrial & Engineering Chemistry Research 44 (2005) 6605–6614.
[69] Y. Wei, D. Zhang, F. Chang, Z. Liu, Catalysis Communications 8 (2007) 2248–2252.
[70] J. Ereña, I. Sierra, M. Olazar, A.G. Gayubo, A.T. Aguayo, Industrial & Engineering Chemistry Research 47 (2008) 2238–2247.
[71] I. Sierra, J. Ereña, A.T. Aguayo, J.M. Arandes, M. Olazar, J. Bilbao, Applied Catalysis B 106 (2011) 167–173.